Hydrodynamic Model of the Martian Atmosphere between Near-Surface Layers and an Altitude of about 130 km

C.-V. Meister, P. Hartogh, G. Villanueva
(Max-Planck-Institut für Aeronomie, Max-Planck-Str. 2, D-37191 Katlenburg-Lindau, Germany)

U. Berger
(Leibniz-Institut für Atmosphärenphysik, Schloß-Str. 6, D-18225 Kühlungsborn, Germany)

In the present work, a general circulation and climate model of a dustless, pure carbon dioxide Martian atmosphere is presented. The model is valid for altitudes between the surface of the planet and the lower thermosphere at about 135 km. Much attention is paid to the parametrization of the energy balance at the surface and to the atmospheric radiation fluxes in the infrared and solar spectra. Between altitudes of 10 km and 120 km, Rayleigh friction and vertical eddy diffusion, caused by internal gravity waves, are considered. At altitudes above 100 km, molecular heat conduction and dynamic viscosity are also taken into account. Thus, in the present state, the model is able to simulate reasonable climatology patterns of winds and temperature fields of different Martian seasons. Using the model, a prediction of the diurnal variations of the surface temperature is possible. First numerical results of the model for the altitudinal and latitudinal dependences of the temperature and the zonal and meridional wind velocities in the Martian atmosphere for summer in the northern hemisphere are obtained and discussed.

1. Introduction

Much of our knowledge of the current global circulation and climate of the Martian atmosphere derives from the spacecraft missions Mariner 9 (see e.g. Conrath et al. 1973) and Viking (see e.g. Wilson and Richardson 2000). Then, the Mars Pathfinder mission helped to determine the vertical structure of the atmosphere at a single site (e.g. Schofield et al. 1997, Haberle et al. 1999). From ground-based mm- and sub-mm observations, altitudinal temperature profiles from 0 - 75 km have been derived (see e.g. Hartogh et al. 1997).

Nowadays, infrared spectra of the Thermal Emission Spectrometer (TES) investigation (6 - 50 μm) on the Mars Global Surveyor (MGS) allow to retrieve latitudinal, longitudinal and seasonal dependences of the atmospheric thermal structure up to altitudes of 65 km (0.01 mbar). Additionally, dust and water ice aerosol optical depths, and water vapour column abundances have been determined (Smith et al. 2001). The MGS experiments also indicate the presence of planetary-scale wave structures (Wilson 2000, 2002).

In near future, new (especially microwave) experiments with higher resolution will be performed which will further strongly improve the knowledge of the structure, dynamics and chemistry of the Martian atmosphere. Air- and spaceborne telescopes as well as limb- and nadir sounders in low Mars orbits will provide highly resolved altitude profiles of temperature, wind, water vapour and minor species from ground to about 130 km altitude and therefore make an important contribution to a better understanding of the general circulation and the climate on short and long time scales. For instance, the experiment MIME (Microwave Investigation on Mars Express) was the first of such microwave sounders. MIME had the capability to spacially resolve the Martian atmosphere by about 5 km in altitude and several 10 km in longitude and latitude (Hartogh 1998).

On the other hand, since already four decades, general circulation and climate models designed for the Earth have been adapted to Mars (e.g. Leovy and Mintz 1969; Hourdin et al. 1993; Wilson et al. 1996; Forget et al. 1999; Haberle et al. 1993, 1999; Richardson and Wilson 2002a). These models take into account such peculiarities of the Martian atmosphere as the strong influence of the interaction between the surface of the planet and the atmosphere, the seasonal variations of the circulation by the changes of the dimensions of the polar caps and the amount of carbon dioxide ice, as well as the occurrence of dust storms of different intensities and dimensions. But the quantitative description of these phenomena has yet to be improved. Especially, after the MOLA (Mars Orbiter Laser Altimeter) experiment (e.g. Bills and Nerem 2001), recently much effort has been made to improve essentially the topographic description of the planet (Forget et al. 1999; Richardson and Wilson 2002a).

Further, all the Martian models base on terrestrial climate models. They all describe the heating by solar and infrared radiation, and they take the surface energy balance into account. But, usually, they describe atmospheric processes up to altitudes above the Mars surface not heigher than 95 km. Thus, here the new atmospheric model Mart-ACC (Martian Atmosphere - Circulation and Climate) is presented that gives a reasonable description of the atmosphere up to 135 km altitude. The basis of this model forms the Cologne Model of the Middle Atmosphere (COMMA), which was developed for the Earth's middle atmosphere between 10 km and 120 km (Ebel and Berger 1997).

2. Basic system of hydrodynamic equations

As the Martian atmosphere is optically rather thin concerning the solar radiation, it is mainly heated from the surface of the planet. Thus, a vertical temperature gradient exists. Besides, the solar energy is mainly absorbed at lower latitudes, and not at the poles, which results in a horizontal temperature gradient. Further, because of the rotation of the planet, a Coriolis force and a comparatively small centrifugal force exist.
Thus, neglecting the action of the centrifugal force, the following system of hydrodynamic equations is considered (Holton 1975):
zonal momentum balance:

$$\frac{\partial u}{\partial t} = -\frac{1}{r\ \cos\varphi}\frac{\partial u^2}{\partial \lambda} - \frac{1}{r\ \cos\varphi}\frac{\partial}{\partial \varphi}(uv\ \cos\varphi) - \frac{1}{\rho_o}\frac{\partial}{\partial z}(\rho_o w u)$$
$$+\left(f + \frac{u}{r}\ \tan\varphi\right) v - \frac{1}{r\ \cos\varphi}\frac{\partial \Phi}{\partial \lambda} + X, \tag{1}$$

meridional momentum balance:

$$\frac{\partial v}{\partial t} = -\frac{1}{r\ \cos\varphi}\frac{\partial (uv)}{\partial \lambda} - \frac{1}{r\ \cos\varphi}\frac{\partial}{\partial \varphi}(v^2\cos\varphi) - \frac{1}{\rho_o}\frac{\partial}{\partial z}(\rho_o w v)$$
$$-\left(f + \frac{u}{r}\ \tan\varphi\right) u - \frac{1}{r}\frac{\partial \Phi}{\partial \varphi} + Y, \tag{2}$$

vertical hydrostatic balance:

$$\frac{\partial \Phi}{\partial z} = \frac{RT}{m^* H}, \tag{3}$$

continuity of mass:

$$\frac{1}{r\ \cos\varphi}\frac{\partial u}{\partial \lambda} + \frac{1}{r\ \cos\varphi}\frac{\partial}{\partial \varphi}(v\ \cos\varphi) + \frac{1}{\rho_o}\frac{\partial (w\rho_o)}{\partial z} = 0, \tag{4}$$

thermodynamic relation between diabatic heating and potential temperature:

$$\frac{\partial T}{\partial t} = -\frac{1}{r\ \cos\varphi}\frac{\partial (uT)}{\partial \lambda} - \frac{1}{r\ \cos\varphi}\frac{\partial}{\partial \varphi}(vT\ \cos\varphi) - \frac{1}{\rho_o}\frac{\partial}{\partial z}(\rho_o w T) + \frac{RwT}{m^* c_p H} + \frac{\kappa J}{H} + Q. \tag{5}$$

In the horizontal momentum balances eqs. (1, 2) spherical coordinates (λ, φ, r) are used, with λ - geographical longitude, φ - geographical latitude, and r - the radial distance which is approximated by the radius of the planet.

$$f = 2\Omega\ \sin\varphi \tag{6}$$

is the Coriolis factor, and Ω ($= 2\pi/T$, T = 24h 39 min 35s) - the angular velocity of the planet. Further, in the horizontal momentum balances the vertical velocity contributions are neglected assuming

$$w\ \cos\varphi \ll v\ \sin\varphi \tag{7}$$

in eq. (1) and

$$\frac{vw}{r} \ll 2\Omega\ |u\ \sin\varphi| \tag{8}$$

in eq. (2). The vertical momentum balance is replaced by the hydrostatic balance, where Φ denotes the planetary potential,

$$\Phi = \int_0^{z^*} g\ dz^* \tag{9}$$

$g = 3.73$ m/s^2 is the Martian gravitational acceleration. The measure of the altitude above the surface of the planet is designated by $z = -H\ln(p/p_s)$, $H = RT_s/g \approx 10$ km is the scale height, $R/m^* = 192$ J/(kg·K) - the specific gas constant of the dry Martian air. T_s determines a constant mean temperature, $T_o = T_o(z)$ a local mean temperature, and T - the departure from $T_o(z)$. Analogously, p is the pressure, and p_s and ρ_s are a constant reference pressure and a constant reference density respectively.

$$\rho_o(z) = \rho_s \exp(-z/H) \tag{10}$$

describes an altitudinal dependent mean atmospheric density. u designates the eastward zonal wind velocity, v - the northward meridional wind velocity, and $w = dz/dt$ - a measure of the vertical wind velocity. X, Y and Q are friction terms.

$$X = -\alpha_R u + K_{zz}\frac{\partial^2 u}{\partial z^2} + \nu\frac{\partial^2 u}{\partial z^2}, \tag{11}$$

$$Y = -\alpha_R v + K_{zz}\frac{\partial^2 v}{\partial z^2} + \nu\frac{\partial^2 v}{\partial z^2}. \tag{12}$$

Q is the sum of the diabatic heating rate Q_R and an additional diffusive heating term F_T

$$Q = Q_R + F_T, \tag{13}$$

$$Q_R = \frac{J_{sol}}{c_p}\exp\left[\frac{\kappa z}{H}\right] + \frac{J_{ir}}{c_p}\exp\left[\frac{\kappa z}{H}\right]. \tag{14}$$

c_p defines the specific heat at constant pressure, and $\kappa = R/c_p$. The main diabatic heating source is the absorption of solar radiation. The main absorption band of carbon dioxide lies in the 2.7 μm region. In a plane parallel atmosphere, for the solar radiation flux S_ν under the zenit angle θ_o in the spectral interval $\Delta\nu$, one has a radiation intensity of

$$J_{sol} = \frac{-\mu S_\nu}{\rho(z)}\frac{d}{dz}\left(\exp\{-\tau_\nu(z)/\mu\}\right), \quad \tau_\nu(z) = \int_z^\infty k_\nu(z)\rho(z)\ dz, \quad \mu = \cos(\theta_o). \tag{15}$$

In case of the solar spectrum, the optical depth τ_ν may be presented by

$$\tau_\nu = k_\nu(p_o, T_o)\int\left(\frac{p}{p_o}\right)^n\left(\frac{T_o}{T}\right)^m du^*, \tag{16}$$

where $u^* = \int \rho\ dz$ is an effective column, $p_o = p_o(T_o)$, and n=1.75 and $m = 8 - 11$ in case of carbon dioxide (Stephens 1984). The solar energy flux at the 2.7 μm absorption band amounts to about 3 % of the total solar energy. Thus, further the dependence of the absorption function A_ν on the spectral interval $\Delta\nu$ given by Liou and Sasamori (1975) is taken into account

$$A_\nu = \frac{A}{\Delta\nu} = \frac{1}{\Delta\nu(C + D\log(x + x_o))}, \quad x = yp^{K/D}, \quad x_o = 10^{-C/K}. \tag{17}$$

The values of the constants C, D and K are found empirically and tabulated in Liou (1980).
The spectral intensity of the infrared emission J_{ir} is expressed by

$$J_{ir} = \frac{\pi}{\rho_o(z)}\Big[-B_r(z)\frac{dT_\nu(z,\infty)}{dz} - [B_r(0) - B_r(z)]\frac{dT_\nu(z,0)}{dz} \tag{18}$$

$$-\int_0^z [B_r(z^*) - B_r(z)]\frac{\partial^2 T_\nu(z,z^*)}{\partial z\partial z^*} - \int_z^\infty [B_r(z^*) - B_r(z)]\frac{\partial^2 T_\nu(z,z^*)}{\partial z\partial z^*}\Big],$$

where

$$T_\nu(z, z^*, \mu) = 1 - A_\nu(z, z^*, \nu) = \exp\left[-\frac{1}{\mu}\int_z^{z^*} k_\nu(p,T)\rho_a\ dz\right] \tag{19}$$

is the diffuse transmission in the frequency interval $d\nu$, $B_r = \int d\nu\ B_\nu$. B_ν describes the Planck source function, that means, in the present model the atmosphere is considered to be in local thermodynamic equilibrium. The absorption function A_ν in eq. (18) for carbon dioxide is calculated from (Ramanathan 1976)

$$A_\nu = A_o u^*[1 - 0.18u^*/\delta] \text{ for } u/\delta \le 1.5, \tag{20}$$

$$A_\nu = 0.753A_o\delta\left[\ln(u^*/\delta)^{3/2} + 1.21\right] \text{ for } u/\delta \ge 1.5.$$

$u^* = S\beta w^*/A_o$ is a dimensionless optical depth of the column w^* of the absorber in atm·cm, and the line parameters $\delta = a\pi^{1/2}\alpha_D/d$ with $a = 2$, $\alpha_D = 3.6\cdot 10^{-5}T^{1/2}$ cm^{-1}, $S = 194$ cm^{-2}atm^{-2}, and $d = 156$ cm^{-1}. The first term on the right side of eq. (18) describes the loss of infrared radiation to space, the second term describes the exchange of heat between surface and atmosphere, and the last two contributions take the radiation flux between different

layers of the atmosphere into account. Mostly, only the first term on the right side of eq. (18) is considered and approximated by the Newtonian cooling law. The friction term F_T reads

$$F_T = \lambda \frac{\partial^2 T}{\partial z^2} + \frac{1}{P_T \rho} \frac{\partial}{\partial z} \rho K_{zz} \left(\frac{\partial T}{\partial z} + \Gamma \right), \tag{21}$$

where Γ designates the adiabatic temperature gradient of dry air and $P_T \approx 3$ is the turbulent Prandtl number.

$$\alpha_R = \alpha_o \exp\{z/c\}, \quad \text{with} \quad z = \ln(p_o/p), \quad c = 2.5, \quad p_o = 610 \text{ Pa}, \quad \alpha_o^{-1} = 30\ d \tag{22}$$

(analogous to the work of Schoeberl and Strobel (1978) for the Earth's climate) is the Rayleigh friction coefficient,

$$\nu = 3.643 \cdot 10^{-8} (T - 273.15\text{K}) + 1.37 \cdot 10^{-5} \quad \text{in [kg/m} \cdot \text{s]} \tag{23}$$

represents the dynamic viscosity of pure carbon dioxide and,

$$\lambda = 7.85 \cdot 10^{-5} (T - 237.15 \text{ K}) + 1.45 \cdot 10^{-2} \quad \text{in [W/(m} \cdot \text{K)]} \tag{24}$$

- the molecular heat conductivity of pure carbon dioxide. Both coefficients ν and λ are given by linear approximations of data taken from tables (D'Ans-Lax 1967).

$$K_{zz} = \frac{k(\hat{u} - c_{ph})^4}{N_{BV}^3} \left(\frac{1}{2H} - \frac{3}{2} \frac{\hat{u}_z}{(\hat{u} - c_{ph})} \right) \tag{25}$$

is the vertical eddy diffusion coefficient (Lindzen 1981). In equation eq. (25), k designates the horizontal wave number of internal gravity waves, c_{ph} is the horizontal phase velocity of these waves, $\hat{u}$ and $\hat{u}_z$ are the mean zonal wind velocity and the corresponding wind shear, and N_{BV} is the Brunt-Väisälä frequency,

$$N_{BV}^2 = \frac{g}{H} - \frac{g^2}{c_s^2}, \quad c_s^2 = \frac{\gamma p}{\rho}. \tag{26}$$

3. Numerical solution

The system of equations (1-5) is solved numerically using the leapfrog-scheme, which is a dissipative method of second order with respect to spatial and time steps (Dautray and Lions 1990). Solutions of the leapfrog-scheme are further corrected introducing after forty eight leapfrog steps three steps within the dissipative Euler backward scheme (Ebel and Berger 1997). The integrations are performed using a time step of 100 seconds. The solutions extend from the ground of the Martian atmosphere through the lower and middle atmosphere, up to altitudes of the lower thermosphere of 135 km (in log-pressure coordinates, what corresponds to about 150 km in geometrical altitude), exceptionally using a vertical grid refinement of $\Delta z = 1$ km. Thus the model is able to resolve tidal wave layers in the upper Martian atmosphere. The horizontal resolution of the numerical model is given by a 5^o latitude versus 5.625^o longitude grid.

First solutions of the present model Mart-ACC for a dustless, pure carbon dioxide atmosphere and summer on the northern hemisphere ($Ls = 90^o$) using a smoothed topography (Fig. 1) are presented in Figs. 2-4. For the latitudinal resolution a value of $5^o \approx 148$ km is chosen, and the longitudinal resolution of the results equals only $22.5^o \approx 475$ km. Paying the main attention to the improvement of the numerical model for higher-altitude regions in this work, the consideration of a smoothed topography is a reasonable approximation. The actually used topographic data have maximum altitudinal differences of 2 km (Fig. 1), and, besides, these data are yet multiplied by a factor 0.2 to accelerate the numerical calculations. Here it should be mentioned that the highest shield volcano of the Mars, the Olympus Mons, has an altitude of about 27 km and a diameter of more than 600 km at the planetary surface (Tanaka et al. 1992).

Starting the integration of the hydrodynamic system of equations eqs. (1-5) at $t = 0$ s with an isotherme atmosphere ($T = 160$ K) heated (mainly via the planetary surface) by solar radiation, after about 20-25 sols an equilibrium state of the Martian atmosphere is achieved.

In Fig. 2, the calculated equilibrium values of the surface temperatures are shown as function of geographic latitude and geographic longitude. It is to be seen that, because of the obliquity of the rotation axis of the Mars, a maximum surface temperature occurs at mean latitudes of about 30-40^{o}N at a longitude of 60^o (corresponding to day-time). Along the parallel of 30^{o}N, between day and night a temperature difference of 55 degrees is found. The maximum longitudinal temperature gradients amount to 0.7 K/grad $\approx 10^{-5}$ K/m and the maximum latitudinal temperature gradients equal 1.9 K/grad $\approx 3 \cdot 10^{-5}$ K/m.

Zonal mean values of the temperature in the Martian atmosphere are presented in Fig. 3. Although the surface temperature has a maximum at latitudes of 40^oN (Fig. 2), because of the presentation of the averages over all longitudes, in Fig. 3 the temperature maximum occurs at the North Pole. Then, the temperature decreases in the Martian lower atmosphere ($z \lesssim 50$ km) and in the mesosphere (50 km $\lesssim z \lesssim$ 100 km) before it again slightly increases at the lower border of the thermosphere ($z \approx 100$ km). At an altitude of 135 km it has values of 200 K.

Between 30^oS and 60^oS in the winter hemisphere, strong horizontal temperature gradients occur at altitudes below 20 km. In the summer hemisphere the temperature gradients are almost vertical. Up to an altitude of 20 km (1 mbar), the results of Mart-ACC for the zonal mean temperature compare reasonably well with the results of Pollack et al. (1981) for a dust-free pure carbon dioxide atmosphere at northern summer solstice obtained by the NASA-M model. For larger altitudes, in (Pollack et al. 1981) no results are given. Pollack et al. (1981) also initiate the numerical integration from an isothermal state ($T = 200$ K). The lower boundary of their model equaled about 5 mbar (575 m). But for the contour lines for 150 K and 160 K between 50^oS and 40^oS, they obtain nearly vertical lines.

Above the equator at altitudes of 40 km, a temperature minimum of 131 K occurs in Fig. 3. This, again, is mainly an effect of the presentation of zonal mean values. But, a small local temperature decrease of about 10-15 K in the temperature region of about 150 K is also to be seen in the non-zonally averaged temperature profiles at the equator at altitudes of 30-40 km in the Martian afternoon. The same effect was also found by Forget et al. (Fig. 8 in (Forget et al. 1999)) performing simulations with the LMD-AOPP grid point model during early northern summer. Here it should be underlined that the LMD-AOPP model describes rater well Mars Global Surveyor climate data (Forget et al. 2003). The temperature-minimum phenomenon (even in a dustless model) has to be further studied in future. May be it is a topographic and/or wave effect. Besides, two further temperature minima at altitudes of 100-110 km at $90^o - 50^o$ S and $40^o - 90^o$ N are seen in Fig. 3. These effects seem to be related to tidal wave activity.

The strong temperature gradients in the Martian atmosphere, especially those in the meridional direction, but at lower altitudes also those in longitudinal directions cause a rather strong atmospheric circulation. Calculated zonal mean values of the zonal wind velocity and zonal mean values of the meridional wind velocity as function of latitude and altitude are presented in Fig. 4 and Fig. 5, respectively. The zonal winds in summer on the northern hemisphere are about one order of magnitude larger than the meridional winds. But first results of the seasonal dependence of the circulation obtained by Mart-ACC show, that in spring and autumn the zonal winds are only 2-3 times larger than the meridional winds.

The intensive westward (blue, negative-value) zonal winds in the northern hemisphere (Fig. 4) are caused by the daily-mean northward directed temperature gradients. But, as e.g. the maximum values of the velocity gradients at latitudes of 30^oS - 10^oN and altitudes of 40-50 km reach values satisfying $\partial u/\partial y \approx 5.6 \cdot 10^{-5}$ s^{-1} and $(u/v)\partial v/\partial y \approx 21 \cdot 10^{-5}$ s^{-1}, at maximum atmospheric wind speeds the nonlinear velocity terms in the momentum balance eq. (1) are about four times larger than the Coriolis term $fv \approx 7 \cdot 10^{-5} v$ s^{-1} (the diameter of the Mars equals 6793 km), so that the atmosphere becomes a non-geostrophic one. Here it should be noted, that the zonal wind velocities in the northern hemisphere do not agree quantitatively with the results of the LMD-AOPP grid point model. Although the temperature values agree nearly quantitatively and the general circulation patterns mainly coincide, the zonal winds in the southern hemisphere found by the LMD-AOPP grid point model are more than two times larger in the latitudinal region between 50^oS and 60^oS (Forget et al. 1999, Forget et al. 2003). May be, this is only the effect of dust taken into account by Forget et al. between 50^oS and 60^oS at Ls=90^o (see Fig. 1 in (Forget et al. 2003)).

Further, the strong dependence of the zonal winds on the altitude and latitude allow to conclude, that in the atmosphere baroclinic and barotropic waves are generated.

In the altitudinal dependence of the zonal mean values of the meridional wind velocity (Fig. 5), a change of the wind direction from northward (>1.94 m/s) to southward (up to 80 m/s), and again to northward is found. Also in (Pollack et al. 1981), at the planetary surface northward zonal mean meridional winds of 2-6 m/s were obtained, and for altitudes of 20 km, the simulations gave southward zonal winds with velocities of 5 m/s. This change of wind direction is usually interpreted as a manifestation of the Martian Hadley circulation with one Hadley cell. Richardson and Wilson (2002b) report on a second, very much weaker Hadley cell in summer hemispheres. We cannot conclude the existence of a second Hadley cell from Fig 5. The numerical simulations of Richardson and Wilson were performed with the GFDL general circulation model in an altitude region of 0 - 40 km (up to 10 Pa = 0.1 mbar). But, in the present Mart-ACC work it is found that in summer the upper southward winds may have velocities of 80 m/s at heights of 40 km. Additional Mart-ACC studies of zonal winds at times of equinoxes show that in autumn and spring two Hadley cells with a common region of upstreaming winds appear above the equator.

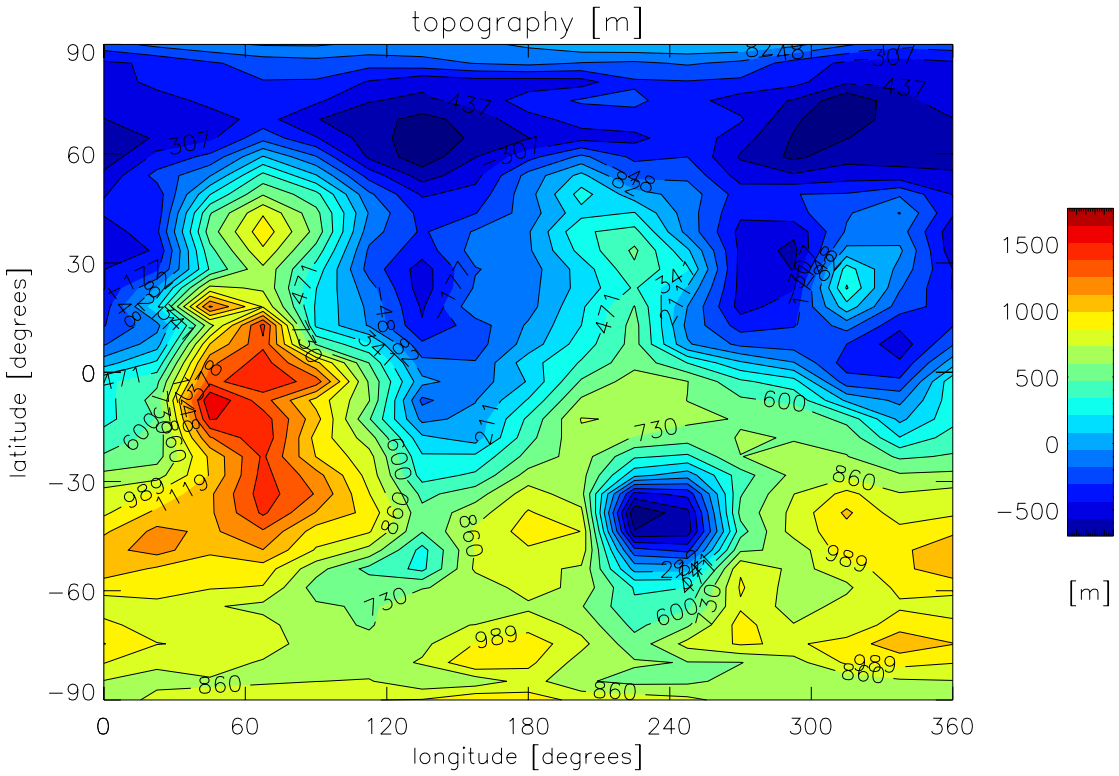

Fig. 1: The smoothed Mars topography only 20 % of which are taken into account in the recent results (Figs. 2-5) of the Mars general circulation and climate model Mart-ACC.

Comparison of recent Mart-ACC with other general circulation models of the Martian atmosphere

Description	NASA AMES [A]	GFDL [B]	LMD and AOPP [C]	Mart-ACC [D]
fully non-linear equations	yes	yes	yes	yes
vertical coordinate z	hybrid	hybrid	log-pressure	log-pressure
steps	30	40	?	118
Δz [km]	0.01-3	2	refined	1.1
lower boundary [km]	0	0.25	0	0.34
upper boundary [km]	95	85	120	135
horizontal grid (lat. × long.)	$5^o \times 6^o$	$3^o \times 4^o$	$4^o \times 6^o$	$5^o \times 5.6^o$
radiation code CO_2 (solar + IR)	yes	yes	yes	yes
surface energy equation	yes	yes	yes	yes
planetary boundary layer + convective adaption	yes	yes	yes	yes
topography	smoothed	MOLA	(MOLA)	smoothed
dust	yes	yes	yes	no
CO_2- + H_2O-cycles	no H_2O	yes	no H_2O	no
non-LTE radiation transport	partly	no	partly	no
gravity wave parame-trization	no	no	yes	yes
molecular heat conduction	no	no	no	yes
dynamical viscosity	no	no	no	yes

[A] NASA AMES = Ames Research Center, California (Haberle et al. 1999),
[B] GFDL = SKYHI, NOAA Princeton (Richardson and Wilson 2002),
[C] LMD and AOPP = Laboratoire de Météorologie Dynamique, Paris and Department of Atmospheric, Oceanic and Planetary Physics at Oxford University (Forget et al. 2003),
[D] Mart- ACC = Cologne University (Ebel and Berger 1997).

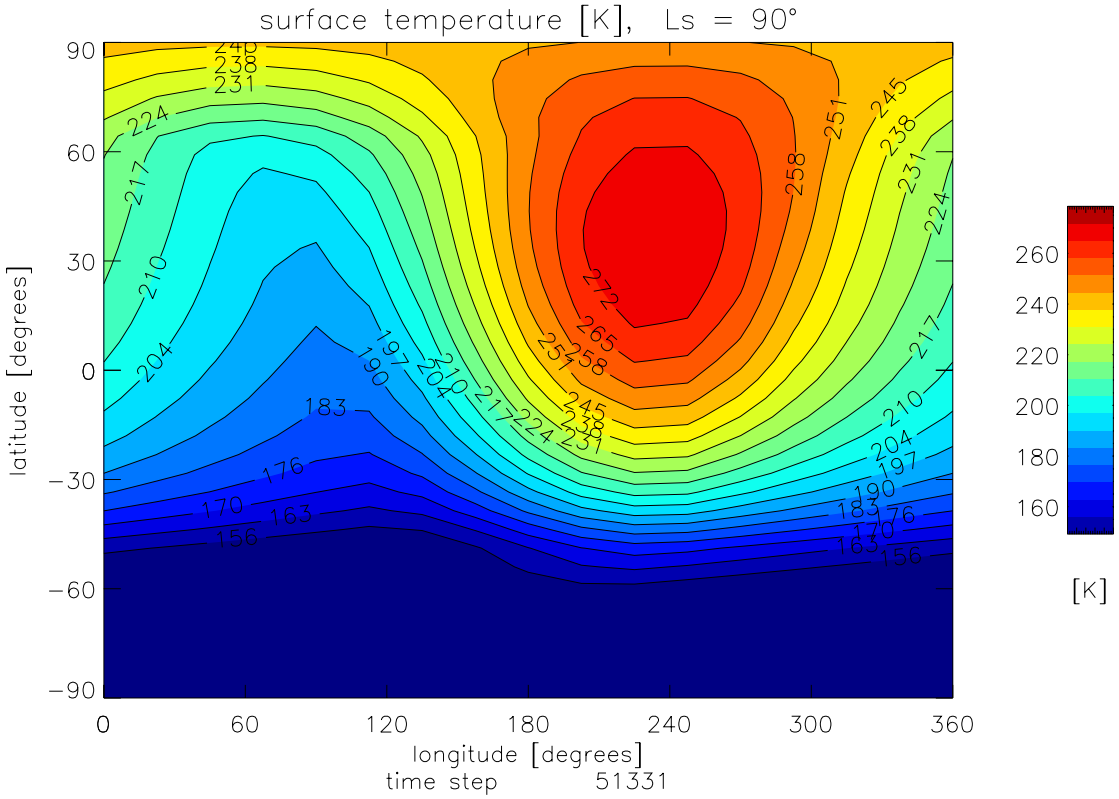

Fig. 2: Mean surface temperature calculated for summer on the northern hemisphere using Mart-ACC, $L_s = 90^o$.

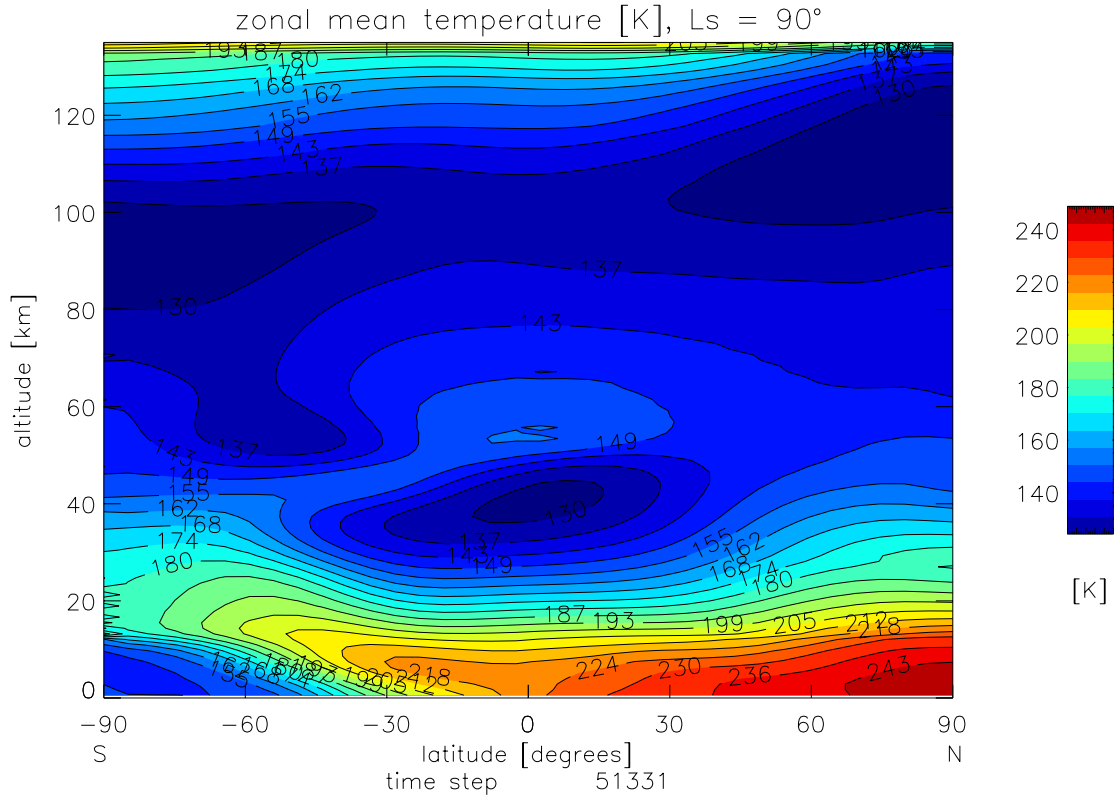

Fig. 3: Zonal mean temperature calculated for summer on the northern hemisphere using Mart-ACC, $L_s = 90^o$.

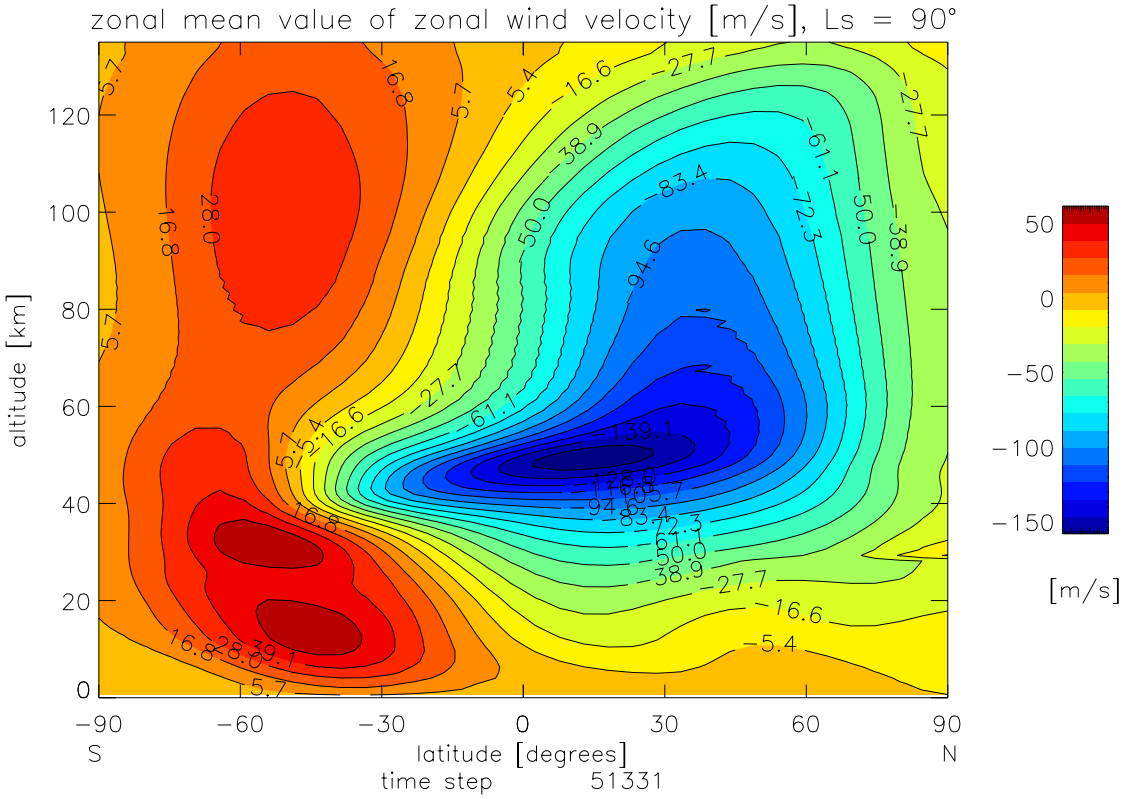

Fig. 4: Zonal mean value of zonal wind velocity calculated for summer on the northern hemisphere using Mart-ACC, $L_s = 90^o$.

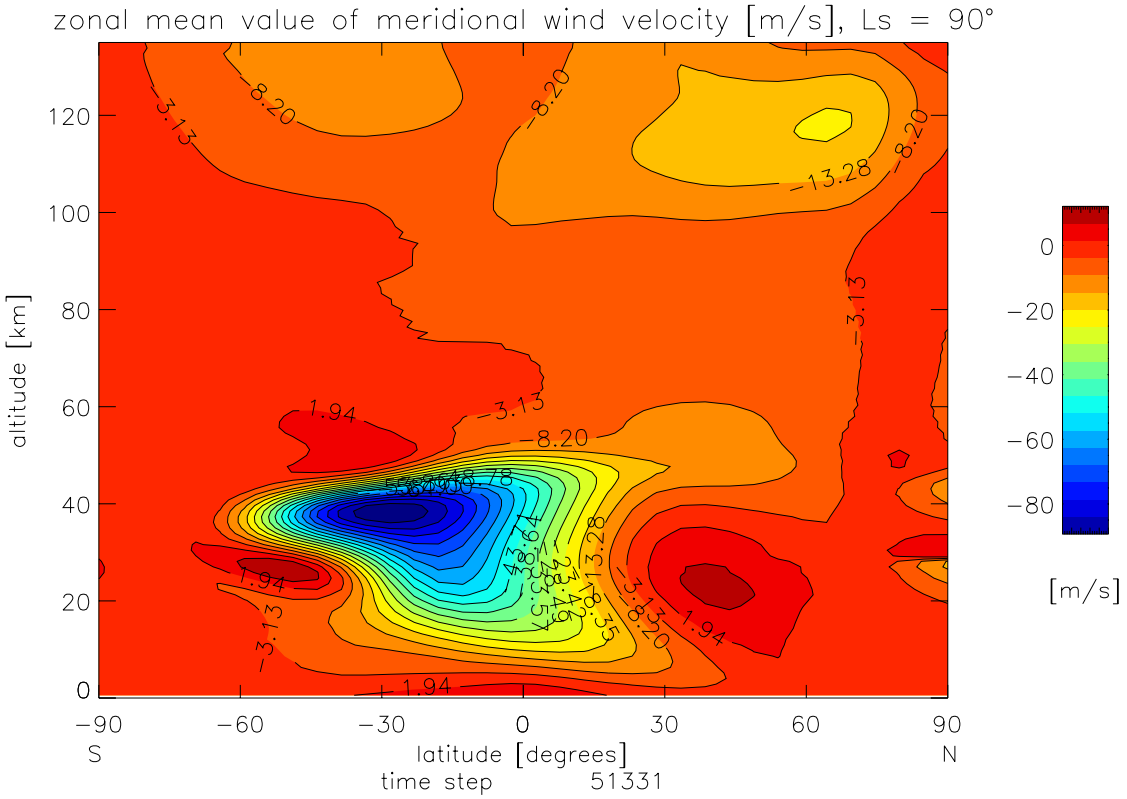

Fig. 5: Zonal mean value of meridional wind velocity calculated for summer on the northern hemisphere using Mart-ACC, $L_s = 90^o$.

4. Conclusions

A rather complex, fully-nonlinear, three-dimensional general circulation and climate model for the Martian atmosphere without dust has been developed taking into account a smoothed topography.

The application of the smoothed topography means that the excitation of gravity waves by mountains is not adequately taken into account in the developed model, and thus the description of the dynamics of the lower and middle atmosphere of the Mars has yet to be improved.

The main advantage of the circulation and climate model presented here is that it describes the Martian atmosphere up to large altitudes of 135 km, while other important models, besides the LMD-AOPP model (Forget et al. 2003), give only results up to 95 km (see Table 1). So, in comparison with other models (see Table 1), for heights between 10 km and 120 km, Rayleigh friction and vertical eddy diffusion caused by internal gravity waves, are considered. Besides, at altitudes above 100km, also molecular heat conduction and dynamic viscosity are taken into account. Thus, to accelerate the enormous numerical calculations it is reasonable to introduce first a smoothed topography.

Further, about half of the Martian year, the atmosphere of the Mars may be considered to be dustless. Thus, also the neglection of near-surface and atmospheric dust is a useful approximation to obtain quickly numerical results.

Nevertheless, much attention is also paid in the Mart-ACC model to the surface energy balance, to its heating by solar radiation and its cooling by infrared emissions and heat convection. Thus, using the model, a prediction of the changes of the surface temperature with the daytime is possible.

The results for the mean zonal temperature reflect the existence of the lower, middle and upper atmospheres of the Mars as they should occur in accordance with the US Martian standard atmosphere by Seiff and Krik presented in 1977 (see e.g. the review by Zurek (1992)).

Further, in the present paper the radiation transport within the carbon dioxide atmosphere is assumed to proceed within local thermodynamic equilibrium (LTE). But, in the middle atmosphere, at altitudes of 45 km to 110 km, collisions between the carbon dioxide molecules become too infrequent to maintain local thermodynamic equilibrium (LTE) for the major CO_2 vibrational bands. Lopez-Valverde (1998) showed that non-local thermodynamics may be roughly taken into account in the solar heating rates multiplying the rates by a factor $f = (2.2 \cdot 10^4 \text{ p})/(1+2.2 \cdot 10^4 \text{ p})$ (p in mbar). That means $f \approx 0.7$ at 100 nbar, and $f \approx 0.3$ at 20 nbar. Up to now, no analogeous approximate factor seems to be found for the infrared cooling in the Martian atmosphere. However, the transfer of thermal radiation in the atmosphere dominated by the 15 μm vibrational fundamental band of CO_2 can be approximately described within LTE up to altitudes of 90 km (Bougher and Dickinson 1988). Nevertheless, the refurbishment of Mart-ACC by a state-of-the art non-LTE radiation transport code seems to be an urgent task for future work.

The numerical results for the temperature profiles obtained by Mart-ACC agree generally, even almost qualitatively, rather well with the solutions of other general circulation models - and thus also with the Viking and Mars Global Surveyor experiments.. The solutions of Mart-ACC for the wind velocities are comparable with other simulation results provided that there is no dust in the atmosphere. Thus, in the present state, the model Mart-ACC is able to simulate reasonable climatology patterns of winds and temperature fields for different Martian season. But the model has yet to be improved refining the temperature and wind velocity simulations in the winter hemisphere in regions with strong temperature gradients. Further, non-LTE effects, dust and trace gases like CO, NO, O_3, hydroxyl radicals and water, as well as a more realistic topography have to be included into the numerical model in future.

This paper contains one part of a contribution on Martian general circulation and climate modeling by U. Berger, P. Hartogh, C.-V. Meister and G. Villanueva on the International Annual Meeting of the German Astronomical Society "The Cosmic Circuit of Matter" at the Technical University Berlin in September 24.-28., 2002.

Acknowledgements: C.-V. Meister gratefully acknowledges financial support of the present work by the "Deutsche Forschungsgemeinschaft" under DFG grant H3261/1-1.

References

Bills B.G., Nerem R.S., Mars topography: Lessons learned from spatial and spectral domain comparisons of Mars Orbiter Laser Altimeter and U.S. Geological Survey data, J. Geophys. Res. 106 (E12), 32915-32925, 2001.

Bougher S.W., Dickinson R.E., Mars mesosphere and thermosphere. I. Global mean heat budget and thermal structure, J. Geophys. Res. 94, 7325-7337.

Conrath B., Curran R., Hanel R., Kunde V., Maguire W., Pearl J., Pirraglia J., Welker J., Burke T., Atmospheric and surface properties of Mars obtained by infrared spectroscopy on Mariner 9, J. Geophys. Res. 78, 4267-4278, 1973.

D'Ans - Lax, Taschenbuch für Physiker und Chemiker, Band 1: Makroskopische physikalisch-chemische Eigenschaften, 3rd edition, Ed. E. Lax, Springer-Verlag, Berlin-Heidelberg-New York, 1967.

Dautray R., Lions J.-L., Mathematical analysis and numerical methods for science and technology, Vol. 6, Evolution problems II, p. 104, 1993.

Ebel A., Berger U., Final report. Martian atmosphere - circulation and climate. Mart ACC, BMBF, 1997.

Forget F., Angelats i Coll M., Wanherdrick Y., Hourdin F., Lewis S., Read P., Taylor F., Lopez-Valverde M., Lopes-Puertas M., Modeling of the general circulation with the LMD-AOPP-IAA GCM: Update on model design and comparison with observations, International Conference "Mars atmosphere modeling and observations", 13-15.01.03, Preliminary program and abstracts on line, 6 pp., 2003.

Forget F., Hourdin F., Fournier R., Hourdin C., Talagrand O., Collins M., Lewis S.R., Read P.L., Huot J.-P., Improved general circulation models of the martian atmosphere from the surface to above 80 km, J. Geophys. Res. 104, 24155-24176, 1999.

Haberle R.M., Pollack J.B., Barnes J.R., Zurek R.W., Leovy C.B., Murphy J.R., Lee H., Schaeffer J., Mars atmosphere dynamics as simulated by the NASA/Ames general circulation model I., The zonal-mean circulation, J. Geophys. Res. 98, 3093-3123, 1993.

Haberle R.M., Joshi M.M., Murphy J.R., Barnes J.R., Schofield J.T., Wilson G., Lopez-Valverde M., Hollingsworth J.L., Bridger A.F.C., Schaeffer J., General circulation model simulations of the Mars Pathfinder atmospheric structure investigation/meteorology data, J. Geophys. Res. 104 (E4), 8957-8974, 1999.

Hartogh P., Jarchow C., Martin R., Ground-based microwave measurements of the martian atmosphere, AGU Fall Meeting Dec. 08-12, 1997, San Francisco, supplement to Eos, Transactions, AGU, Vol. 78, No. 46, F411, 1997.

Hartogh P., Solar system research with microwaves, in: Proceedings of the 32nd ESLAB Symposium: Remote Sensing Methodology for Earth Observations and Planetary Exploration (edited by E. Attema, G. Schwehm, A. Wilson), ESA SP-423, ESA Publ. Div., Noordwijk, 23-32, 1998.

Holton J.R., The dynamic meteorology of the stratosphere and mesosphere, Meteorological Monographs 15(37), American Meteorological Society, Boston 1975.

Hourdin F., Phu Le Van, Forget F., Talagrand O., Meteorological variability and the annual surface pressure cycle on Mars, J. Atmos. Sci. 50, 3625-3640, 1993.

Leovy C., Mintz Y., Numerical simulation of the atmospheric circulation and climate of Mars, J. Atmos. Sci., 26, 1167-1190, 1969.

Lindzen R.S., Turbulence and stress owe to gravity wave and tidal breakdown, J. Geophys. Res., 86, 9707-9714, 1981.

Liou K.-N., An introduction to atmospheric radiation, Academic Press, New York, vol. 26, 1980.

Liou K.-N., Sasamori T., On the transfer of solar radiation in aerosol atmospheres, J. Atmos. Sci., 32, 2166-2177, 1975.

López-Valverde M.A., Edwards D.P., López-Puertas M., Roldán C., Non-local thermodynamic equilibrium in general circulation models of the Martian atmosphere, 1. Effects of the local thermal equilibrium approximation on thermal cooling and solar heating, J. Geophys. Res. 103, 16799-16811, 1998.

Pollack J.B., Leovy C.B., Greiman P.W., Mintz Y., A martian general circulation experiment with large topography, J. Atmos. Sci., 38, 3-29, 1981.

Ramanathan V., Radiative transfer within the earth's troposphere and stratosphere: A simplified radiative-convective model, J. Atmos. Sci., 33, 1330-1346, 1976.

Richardson M.I., Wilson R.J., Investigation of the nature and stability of the Martian seasonal water cycle with a general circulation model, J. Geophys. Res. 107 (E5), 10.1029/2001JE001536, 2002a.

Richardson M.I., Wilson R.J., A topographically forced asymmetry in the martian circulation and climate, Nature 416, 298-301, 2002b.

Schoeberl M.R., Strobel D.F., The zonally averaged circulation of the middle atmosphere, J. Atmos. Sci. 35, 577-591, 1978.

Schofield J.T., Barnes J.R., Crisp D., Haberle R.M., Larsen S., Magalhães J.A., Murphy J.R., Seiff A., Wilson G., The Mars Pathfinder Atmospheric Structure Investigation/Meteorology (ASI/MET) experiment, Science 278, 1752-1758, 1997.

Smith M.D., Pearl J.C., Conrath B.C., Christensen P.R., One Martian year of atmospheric observations by the Thermal Emission Spectrometer, Geophys. Res. Lett. 28 (22), 4263-4266, 2001.

Tanaka K.L., Scott D.H., Greeley R., Global stratigraphy, in: Mars, eds. Kieffer H.H., Jakosky B.M., Snyder C.W., Matthews M.S., The University of Arizona Press, Tucson and London, 345-382, 1992.

Stephens G.L., The parametrization of radiation for numerical weather prediction and climate models, Monthly Weather Review 112, 826-867, 1984.

Wilson R.J., Evidence for diurnal period Kelvin waves in the martian atmosphere from Mars Global Surveyor TES data, Geophys. Res. Lett. 27, 3889-3892, 2000.

Wilson R.J., Evidence for nonmigrating thermal tides in the Mars upper atmosphere from the Mars Global Surveyor Accelerometer experiment, Geophys. Res. Lett. 29 (7), 10.1029/2001GL013975, 2002.

Wilson R.J., Richardson M.I., The Martian atmosphere during the Viking mission, I Infrared measurements of atmospheric temperature revisited, Icarus 145, 555-579, 2000.

Zurek R.W., in: Mars, Comparative aspects of the climate of Mars: An introduction to the current atmosphere, eds. Kieffer H.H., Jakosky B.M., Snyder C.W., Matthews M.S., The University of Arizona Press, Tucson and London, 799-817, 1992.